Free Convection Melting of Ice Spheres

C. R. VANIER and CHI TIEN

Syracuse University, Syracuse, New York

Experimental results have been obtained for heat transfer to melting ice spheres by measuring the rate of change of apparent weight. It is found that the traditional correlation format of Nusselt number against Rayleigh number is satisfactory only for bulk temperatures above 7°C. Average Nusselt numbers obtained from the sphere experiments are closely related to previous theoretical work with vertical flat plates.

The understanding and prediction of heat transfer phenomena near an ice/water interface poses a significant free convection problem. In such a system, the effect of maximum density at 4°C. combines with the motion of the interface and the changing body geometry to render classical solutions of little use. Yet melting bodies of ice are of common occurrence and great interest in meteorology, glaciology, and oceanography. One recent industrial application is a compact emergency cooling system for nuclear reactors which uses several million ice cubes (*2*).

The earliest theoretical study of nonhorizontal ice surfaces melting by free convection was by Merk (*8*) who showed that third-order density polynomials for water could be successfully utilized in the boundary-layer equations. By means of the Von Karman-Pohlhausen integral method, Merk predicted a minimum Nusselt number* for melting spheres at 5.31°C. A brief experimental report by Dumore and co-workers (*4*), together with some results from a 10.2 cm. vertical, nonmelting plate by Ede (*5*), generally supported Merk's analysis.

Using photographic techniques, Tkachev (*13*) found a minimum Nusselt number for melting ice cylinders at 5.5°C. Tkachev was apparently the first worker to notice the peculiar nature of the maximum density boundary layer. It had previously been thought that the major flow direction within the assumed boundary layer would be either upwards or downwards according to the bulk fluid temperature. Tkachev suggested that under certain conditions the boundary layer might be split, having a predominantly upward motion immediately adjacent to the ice surface and a region of downward motion outside this. Subsequent experimental work by Schecter and Isbin (*12*) with an isothermal, nonmelting, vertical plate confirmed the existence of such dual-flow velocity profiles (exhibiting both maximum and minimum values), but the boundary-layer equations as approached either by the Von Karman-Pohlhausen integral method or by the similarity transformation method did not give useful results under these conditions. Schecter and Isbin's work suggested the investigation of transition temperatures between unidirectional and split flow regimes. This suggestion was taken up by Vanier and Tien (*15*) who used an accurate numerical method to solve the similarity equations for a semi-infinite vertical plate at constant temperature (T_w) immersed in an indefinitely large volume of water at bulk temperature T_∞. A new solution is necessary for every combination of T_w and T_∞, and by obtaining several hundred such solutions, the authors were able to map out temperature zones for each flow regime. The split boundary layer was found to be confined to two distinct triangular regions within which the similarity equations become quite intractable. A plate of melting ice ($T_w = 0$°C.) is a special case of this problem,* and theoretical solutions (*8, 15*) have shown the associated heat transfer rates to be closely similar to (but somewhat less than) the nonmelting case.

The present experimental study is intended to relate the numerical flat plate results of Vanier and Tien to a more practical geometry (the sphere) and to consider the effect of changing body shape. Two previous experimental studies have used melting ice spheres (*4, 13*), but detailed results and correlations for the heat transfer under maximum density conditions were not presented. Measurements of this kind can be carried out by continuous photography of the body profile or by apparent weight recordings; the latter technique has been used here because of its simplicity. The chief difficulties were to minimize heat conduction losses within the ice and to properly interpret tiny ($\sim$ .01 g.) noise polluted weight changes.

EXPERIMENTAL DESIGN AND PROCEDURE

The experimental procedures consisted of suspending an internally weighted sphere of ice (uniformly at 0°C.) in water and recording its apparent weight with a sensitive balance.

Consider the general melting body shown in Figure 1. It is readily shown that the rate of change of tension in the support wire is related to the rate of change of volume by

$$\frac{dF}{dt} = -g\,(\rho_l - \rho_s)\,\frac{dV}{dt} \qquad (1)$$

assuming that the fluid drag forces on the melting sphere are negligible.† Let the ice be represented by a sphere of diameter D (the initial diameter is D_0), and let an average coefficient of heat transfer be defined by

$$\frac{dQ}{dt} = \bar{h}\,(T_\infty - T_w)\;(\pi D^2) \qquad (2)$$

where dQ/dt is the overall rate of heat transfer to the ice. Since all of this heat is used in the solid-to-liquid phase change

$$\frac{dQ}{dt} = -\rho_s\,\Delta H_f\,\frac{dV}{dt} \qquad (3)$$

and

* With respect to bulk fluid temperature, T_∞.

* The boundary condition at the wall must be altered.

† Based on flat plate results (*15*), the viscous drag on a 10 cm. plate in water at 20°C. is about 10^{-4} g. wt./cm. width and changes much more slowly than the buoyancy force as the volume decreases.

$$\bar{h} = \left(\frac{\rho_s}{\rho_l - \rho_s}\right)\left(\frac{\Delta H_f}{\pi D^2 (T_\infty - T_w) g}\right)\frac{dF}{dt} \quad (4)$$

For a discrete change in diameter ($D < D_0$)

$$D = \left[D_0^3 - \frac{6\ \Delta F}{\pi g(\rho_l - \rho_s)}\right]^{1/3} \quad (5)$$

The advantage of the method chosen is that the apparent weight curve can be measured with fairly high accuracy. If, however, the body shape changes drastically from that of a sphere, the diameter (and hence the surface area) as calculated from Equation (5) may be appreciably in error. In the work of Van der Burgh (*14*) and Kranse and Schenk (*7*), the rate of melting was obtained from a photographic projection of the sphere.

The melting experiments were carried out with ice spheres having nominal diameters 2, 3, and 4 in. These spheres were frozen from distilled water in thin copper molds consisting of two close fitting hemispherical sections. Attached to the upper hemisphere was a ¼ in. expansion tube through which a small lead sinker could be positioned centrally. The molds were cooled at −10°C. for about 8 hr. in the freezing chamber of a conventional household refrigerator, and after the copper sections were removed, smooth solid spheres of ice were obtained, each with a short length of attached wire.

It was desired to minimize the imbedded weight (because of the limited balance capacity), but for reasons of stability the average sphere density was kept at about 1.3 g./cc. The method of freezing causes dissolved air to segregate towards the sphere center and produces characteristic radial patterns of trapped bubbles. It has been reported by Tkachev (*13*) that such trapped air bubbles in the ice do not have any measurable effect on the liquid-to-solid heat transfer rate. Because of this, and because the outer portion (~ 0.5 cm.) of each sphere was reasonably free of such deformities, no degassing precautions were taken.

Before each sphere was used, its temperature was raised from the freezer value to 0°C. by equilibrating the entire mold in an ice bath at 0.4°C. The 2-in. sphere required 30 min. of warming, and the 4-in. sphere at least 2 hr.; at the end of this period, the molds were readily removed.

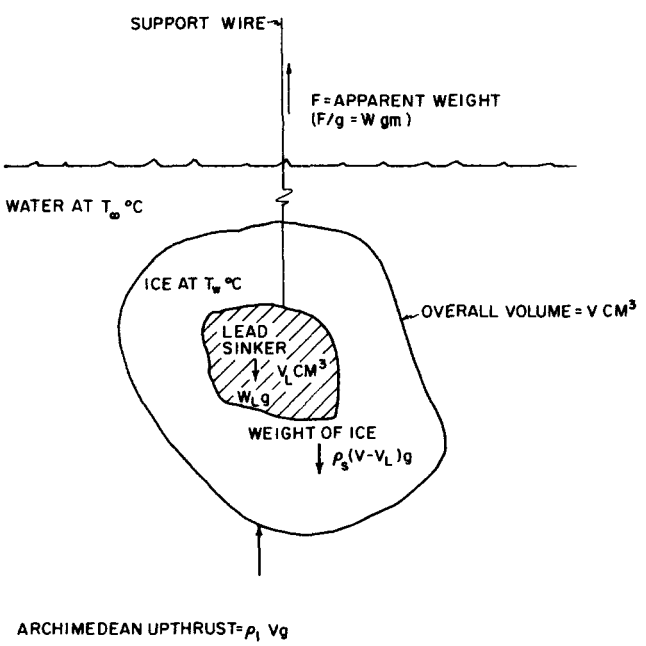

Fig. 1. Force balance on arbitrary body of ice.

The area of a sphere before melting was determined by taking a major and minor circumference measurement with a calibrated length of paper tape. The variation in diameter of a particular sphere was always less than 3%, and errors in area estimation were less than 4%. Previous workers (*14*, *7*) have used thin layers (~ 0.3 cm.) of solid frozen around a cooled mold. The present arrangement allows longer periods of melting to be observed and presents fewer obstructions to the flow, but it requires greater care in achieving a uniform melting temperature.

The melting process was observed in a stainless steel chamber of sufficient size (20 in. × 20 in. × 24 in.) that wall effects were unimportant. Figure 2 shows the arrangement. Temperature control is achieved by means of a cooling coil in a secondary compartment. This allows more uniform temperatures in the observation chamber. Cold water could be circulated from the cooling compartment to the experimental chamber and back. Under measurement conditions, the refrigeration was turned off, the circulation was continued until the two compartments were close to the same temperature (within 0.5°C.), and the liquid was allowed to come to rest.

All experiments were carried out in a room at about 25°C., so that although the tank was uniformly insulated, the mean temperature in the observation chamber rose at about 0.2°C./hr. Three mercury thermometers (with 0.1°C. scale divisions) were evenly stationed around the melting body at depths of 2, 6, and 18 in. and were used to estimate the bulk fluid temperature (T_∞). The deep immersion thermometer reading was weighted twice as heavily as each surface value. If experimental runs were limited to 30 min. or less, the temporal variation in T_∞ was found to be no more than 0.5°C. In assigning a single mean value to T_∞, the error bound is estimated at ±5%. The lowest temperatures were measured with a thermometer having 0.01°C. scale divisions; this was also used for calibration.

An Ainsworth type 15 high speed null-restoring balance was used to measure the weight change of the melting body. The balance has a nominal capacity of 200 g. and can be used with nine weight ranges. The highest of these measures 0 to 25 g., and the lowest measures 0 to 10^{-2} g. The ice sphere was attached to one arm of the balance by a nichrome wire and a light plastic pan for precision analytical weights to the other arm. Since the immersed weight of each unmelted sphere was known to within a few grams, it was possible to equilibrate the two balance arms in a short period of time (about 60 sec.). Any desired scale could then be used to record the weight change. And since only differences in weight are measured, the actual weights in the pan, the weight of the support wire, and the imbedded lead weights can be ignored. For each experimental run, several complete traverses across the

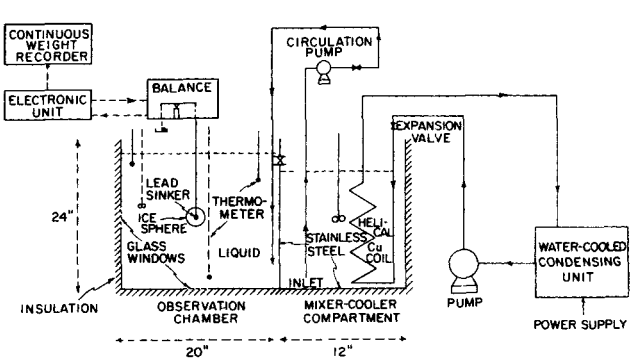

Fig. 2. Schematic diagram of apparatus.

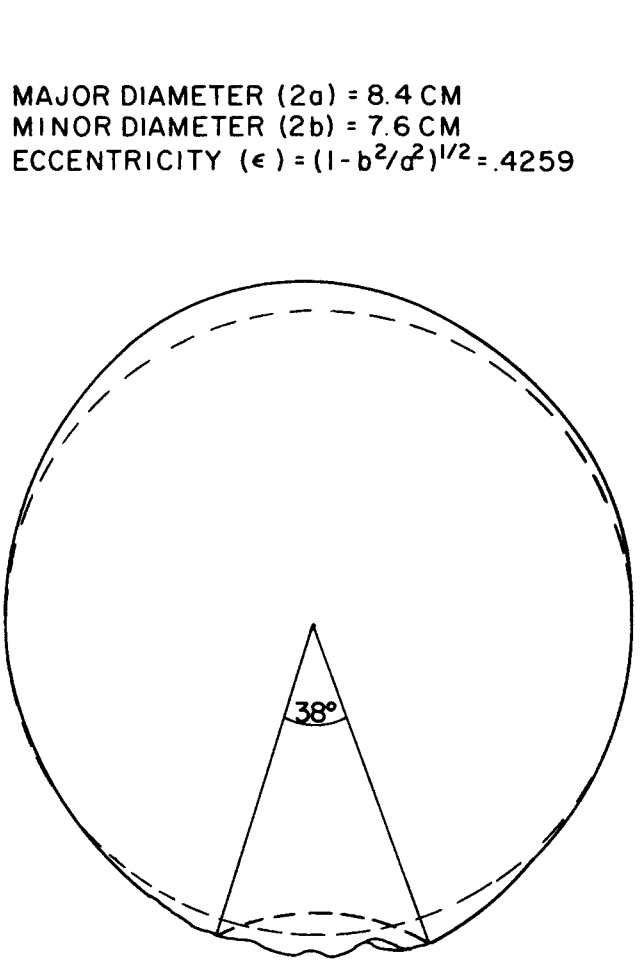

Fig. 3. Profile of melting sphere.

recorder chart were made. At the end of each traverse (full scale on the recorder) a known weight (Fisher certified class S Permas) was added to the pan to restore the recorder output to zero weight difference. The same weight range was used throughout each run. A detailed account of this procedure and the error-correction measures used is given in reference *16*. The controlling error is, of course, introduced by the rate-of-melting data.

TREATMENT OF DATA

Evenly spaced points were taken from the recorder output, and slopes were calculated by central differences, thus generating a melting rate against time curve. Compensation must be made for the following.

Noise

The balance circuit produces rapid oscillations while it is stabilizing, and the best line is drawn by eye through the middle of such oscillations. Low frequency noise is encountered when the balance is at its most sensitive (0.01 and 0.02 g. full scale). This is caused by almost any vibration near the equipment. Fortunately, the melting rate under these conditions ($T_\infty < 4°C.$) is extremely small and practically constant, so a reasonable average value can be found over large time periods.

Lost Time

There is an unavoidable period of lost time at the beginning of each run. Because of this period, there are no weight measurements corresponding to the time when the initial surface area was measured. Since the amount of melting is small, however, an extrapolation can be made to correct the area up to the time of the first reading.

The time derivative of the apparent weight was fitted by least squares, and all subsequent calculations were made on the coefficients of this fit. This allows the necessary extrapolation during the lost time period to be done in a consistent manner. It also tends to smooth out random errors, to facilitate interpolation, and to store the data in a compact form.

Several functions were investigated for the purpose of fitting the data, including the exponential, the quadratic, and the straight line. All of these functions fit equally well, as judged by their standard deviations, and the calculated heat transfer coefficients were entirely within a band width of 2%; therefore, the quadratic was chosen arbitrarily. By integrating this quadratic

$$\frac{\Delta F}{g} = a_0 t + a_1 t^2/2 + a_2 t^3/3 \qquad (6)$$

and hence Equations (4) and (5) were employed to calculate h at each selected time.

The density difference ($\rho_l - \rho_s$) could introduce severe systematic errors, since the two quantities are almost equal. The density of water was evaluated at T_f from (*15*), and the density of ice was taken as 0.9168 ± 0.0005 g./cc. from (*10*). The latent heat of fusion (ΔH_f) at 0°C. was taken as 79.72 ± 0.05 cal./g. from (*11*), and the thermal conductivity of water from 0° to 20°C. was calculated by linear interpolation from (*1*). Table 1* shows heat transfer coefficients calculated by using these properties. Further details are given in (*16*). The Prandtl and Grashof numbers were calculated as in (*15*) by using the instantaneous sphere diameter D. For comparison with data from other sources, it should be noted that $|\beta_\infty|$ will usually be larger than an average coefficient of expansion if $T_\infty > T_w$ and smaller if $T_\infty < T_w$. When T_∞ is very close to 4°C., it is convenient to redefine β_∞, and it has been shown in (*17*) that there is no discontinuity in the heat transfer coefficient at this bulk temperature.

DISCUSSION OF EXPERIMENTAL RESULTS

Change of Shape During Melting

It was observed by Merk (*8*) that a solid sphere becomes pear shaped during free convection melting. The flat plate solution predicts that the major flow direction in the boundary layer is downwards for $T_\infty > 6.1°C.$, and, consequently, a stagnation point should occur at the top of the sphere. For $T_\infty < 4.6°C.$, the flow direction is upwards, and the stagnation point should be at the bottom of the sphere.

To obtain more specific information, sample photographs were taken of the sphere after melting for about 4 min. at 24.5°C. A profile sketch is shown in Figure 3, from which two conclusions can be drawn.

1. For this degree of melting, the geometry approximates well to a prolate spheroid. This can be used to check both the calculation and measurement procedures for determining surface area. The true surface area of the spheroid in Figure 3 (originally a 4-in. sphere) is 194.3 sq.cm. The surface area based on a sphere of the same volume [the assumption of Equation (5)] is 194.0 sq.cm. and the surface area based on a sphere of the same average circumference is 191.3 sq.cm., which is quite satisfactory.
2. At the bottom of the sphere, a circular, scalloped region is hollowed out. The solid angle subtended by the boundary of this incurvation is about 38 deg., which represents 10% of the total surface area. This rather striking

* Tabular material has been deposited as document 00636 with the ASIS National Auxiliary Publications Service, c/o CCM Information Sciences, Inc., 22 W. 34th St., New York 10001 and may be obtained for $1.00 for microfiche or $3.00 for photocopies.

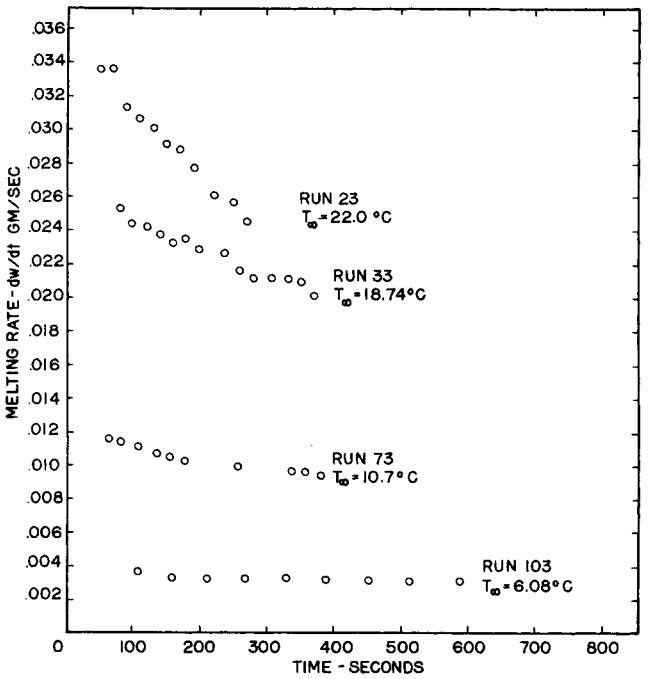

Fig. 4. Raw data: rate of change of apparent weight for 3-in. sphere.

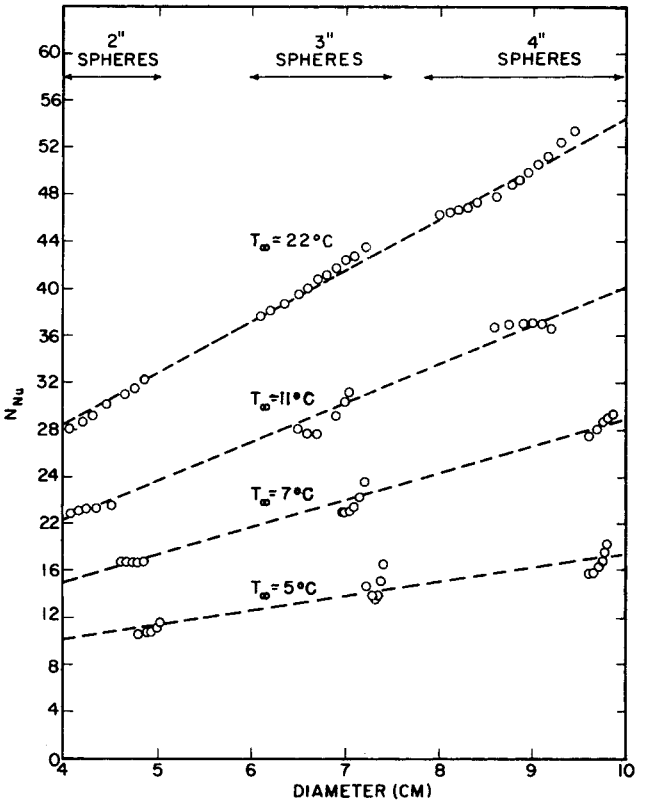

Fig. 5. Variation of Nusselt number with diameter at fixed T_∞.

phenomenon is presumably caused by heavy circulation in the wake of the boundary-layer flow. Kranse and Schenk (7) found a minimum value in local heat transfer coefficient at 140 to 150 deg., which they interpreted as the separation point. The edge of the hollow occurs just after this, at about 160 deg. At greater angles there is a sharp increase in the heat transfer, as evidenced by the concavity.

It is interesting to note that the boundary-layer solutions for curved surfaces do not apply in this region (beyond separation) because the boundary-layer thickness becomes very large and the effects of eddies and conduction parallel to the flow can no longer be ignored. In particular, recent theoretical studies (3, 6) predict zero Nusselt numbers at separation and negative values thereafter. Thus, their overall value for N_{Nu} must be based solely on the heat transfer preceding separation. It is sometimes argued (6) that the contribution of the separated region to the total heat transfer is small. This investigation would imply otherwise.

Melting Curves

Figure 4 presents sample raw data (unsmoothed) for the 3-in. sphere in terms of change of apparent weight (dw/dt) against time. As the area for heat transfer gets smaller, this derivative decreases almost linearly.

Transients of two general types are worth considering.

1. Short term transients. This would include all disturbances in the liquid due to the immersion process. It also includes the establishment of thermal and velocity boundary layers. Provided the sphere is slowly introduced, it is expected that this type of transient will damp out within 30 to 60 sec., owing to the low heat capacity of the boundary layer.

2. Long term transients. These are due to the motion of the ice/water interface. From one point of view, the system is permanently in an unsteady state owing to the changing shape and the changing velocity and temperature distributions relative to some fixed point. This is a matter of definition.

In the theoretical calculations of (15), it was implicitly assumed that relative to the interface position at any particular moment the system was quasi-steady state. The point at issue is whether or not the long-term transients are sufficiently weak for the heat transfer coefficient as formulated in Equation (4) to be independent of particular initial conditions (D_0, t_0). If this condition is satisfied, the results for several different initial sphere sizes should correlate well, and the resulting Nusselt numbers can be freely associated with other dimensionless groups, so that time is relegated to the status of an implied variable. If the condition is not satisfied, it might be found that two spheroids of equal surface area under the same temperature driving conditions had different melting rates according to their past history.

The indicated test cannot be properly applied because the melting data does not overlap at any points. The experimental setup rules out such overlap, because if any melting sequence is allowed to continue for too long, variations in T_∞ will become marked. The 1-in. differential in sphere diameters was chosen to cover an appropriate Grashof number range, and it is never feasible to melt more than 0.5 in. of ice. Figure 5, however, shows the variation of Nusselt number with diameter at several approximately equal temperatures, and it is felt that, despite the scatter, there are no strong transient effects.

Rayleigh Number Correlation

Table 2* shows several least-squares fits based on the semiempirical equation:

$$N_{Nu} = 2 + C\,(N_{Pr} \cdot N_{Gr})^{1/4} \qquad (7)$$

The experimental results fall naturally into two temperature ranges. Data taken with $T_B > 7$°C. appear unaffected by the inversion effects, and the best value for C is 0.422 ± 0.006 in the range $1.7 \times 10^6 < (N_{Pr}N_{Gr}) < 2.4 \times 10^8$. This is shown as curve b in Figure 6. Data taken with $T_\infty < 7$°C. shows about the same value of C but considerably more scattering (twice the standard deviation). This suggests that at least one additional parameter (for example, T_∞) is needed to describe heat transfer under these conditions. The best that can be done with

* See footnote on p. 78.

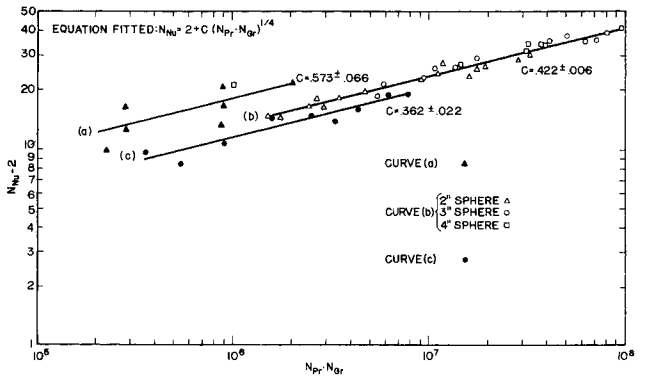

Fig. 6. Nusselt number against Rayleigh number.

the low temperature data in terms of a Rayleigh number is to separate the positive and negative deviations. Nusselt numbers for $T_\infty < 3.6°C.$ are higher than expected and are shown as curve a in Figure 6. Nusselt numbers for $4.8 < T_\infty < 7.1$ are too low (curve c).

In order to check the one-quarter power assumption of Equation (7), a two-parameter fit was carried out, resulting in

$$N_{Nu} = 2 + 0.437\ (N_{Pr} \cdot N_{Gr})^{0.248} \tag{8}$$

which is an excellent corroboration.

Kranse and Schenk (7) have found

$$N_{Nu} = 2 + 0.59\ (N_{Pr} \cdot N_{Gr})^{1/4} \tag{9}$$

to be representative of the nonmelting case and also of the analogous free convection mass transfer from spheres. Their data were obtained from melting experiments on benzene spheres which they corrected by about 8% using Merk's Z factor (8). By removing this added correction, the fitted constant of Equation (9) becomes 0.54, which is in approximate agreement with Tkachev's result (13) for melting spheres of ice ($T_\infty > 15°C.$).

For comparison, the Grashof numbers used in this study were recalculated by using an arithmetic mean temperature basis of T_∞, and the constant was found to be 0.52 for temperatures above 14°C. This constitutes satisfactory agreement, but it should be observed that from the experimental viewpoint there is no strong confirmation that melting lowers the heat transfer rate. Tkachev concluded that to a first approximation it did not, and certainly a factor of ±5% is unlikely to perturb the design engineer.

Returning to the question of transient effects, the results of each experimental run were divided into initial data, corresponding to the smallest time used (t_1), and final data, corresponding to the largest time used (t_2). If transient effects are important, the two batches of heat transfer data come from different statistical populations, and either their mean values, their standard deviations, or both should show significant differences. This hypothesis is not supported by the least-squares fits of Table 2,* which is further evidence that transient effects are unimportant as far as gross system variables, such as Nusselt number, are concerned.

Degree of Melting

Characterization of the extent of melting can be accomplished by considering a small time period, t sec., and a thin uniform melted layer, $\epsilon D_0/2$ cm. If the change in radius is very small ($\epsilon << 1$)

$$\bar{h} = N_{Nu}\frac{k}{D_0} \simeq \frac{\rho_s \Delta H_f\ \epsilon D_0/2}{\Delta T\ t} \tag{10}$$

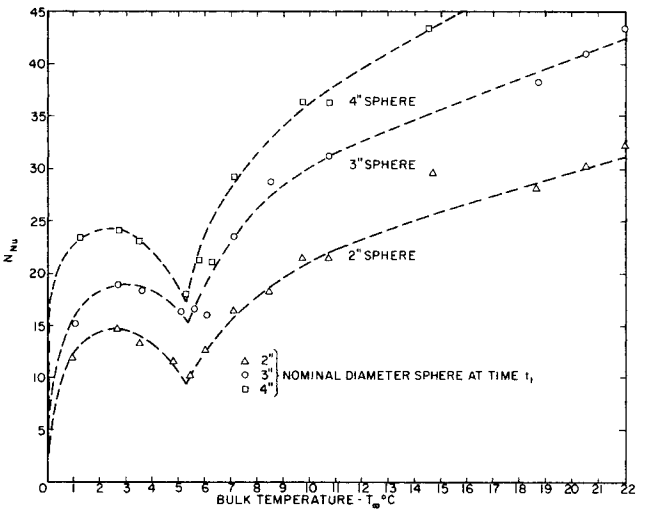

Fig. 7. Nusselt number variation with temperature for approximately constant diameters.

then

$$t \simeq \frac{D_0^2}{(\rho_l/\rho_s)\,(k/\rho_l\ C_p)\ |C_p\ \Delta T/\Delta H_f|\ N_{Nu}} \left(\frac{\epsilon}{2}\right) \tag{11}$$

It is convenient to introduce a new dimensionless group Φ, which is defined as

$$\Phi = N_{Fo\gamma}|M|N_{Nu} = \left(\frac{\bar{h}\ \Delta T\ t}{\rho_s D_0 \Delta H_f}\right) \tag{12}$$

Equation (11) then becomes

$$\Phi = \epsilon/2 \tag{13}$$

The quantity Φ can thus be identified with the degree of melting, and it is suggested that even for large extents of melting, the value of Φ is completely determined by the value of ϵ. The equality (13) applies in the limit of small time, and $\Phi < \epsilon/2$ applies to nearly spherical bodies at all other times. The form of Φ was deduced by Merk (without γ) from boundary-layer relations (8) and by Tkachev from dimensional analysis (13). Its interpretation in terms of ϵ appears to have been unnoticed.

The importance of Φ is its invariant nature; it should not be much affected by the shape of the melting body or by anomalous melting conditions. Table 1* shows the variation of Φ over the present set of experiments. It is seen that all the results have been obtained for $\Phi < 0.094$, and that Equation (13) holds for radial changes of up to 20%. It is claimed by Tkachev that $\Phi = 0.305$ gives complete melting ($\epsilon = 1$) for spheres and cylinders. This is very convenient for design purposes, because once the exact relation of Φ to ϵ has been determined, Equations (7) and (12) can be rapidly used to calculate the time for any desired degree of melting.

The mass transfer counterpart of Φ for rising bubbles of pure gas A in a liquid B would be

$$\Phi = \left(\frac{\Delta C\ D_{AB}\ t}{\rho_g\ D_0^2}\right) N_{Sh} \tag{14}$$

Again, the Φ against ϵ curve plus knowledge of the Sherwood number might be used to calculate the time needed for any desired fraction of mass transfer.

By way of contrast, the time for a given degree of melting could also be found by integrating Equation (4) with $\bar{h}$, known as a *function of diameter*, from Equation (7). The time required to melt from diameter D_0 to D is given

* See footnote on p. 78.

* See footnote on column 1.

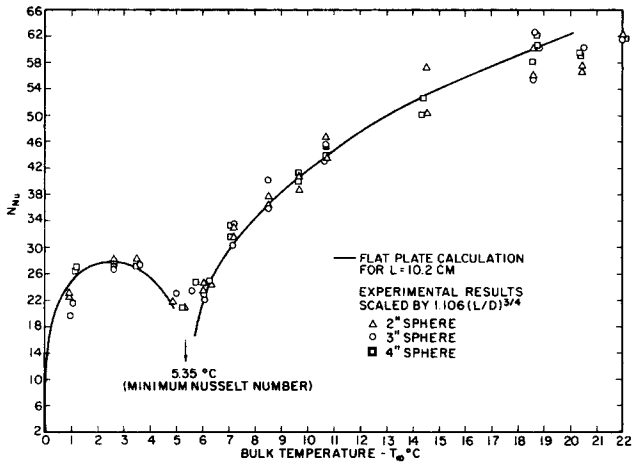

Fig. 8. Correspondence between the melting of flat plates and spheres of ice.

by

$$t = -\frac{1}{b_1}\int_{D_0}^{D}\frac{D}{2 + b_2 D^{3/4}}\,dD \qquad (15)$$

where

$$b_1 = \frac{2\ k\ \Delta T}{\rho_s\ \Delta H_f}, \quad b_2 = C(N_{Pr}N_{Gr}/D_0^3)^{1/4} \qquad (16)$$

In this case, knowledge of the Φ against θ curve would be be replaced by information about the constant C over the whole range of melting.

Correlation with Flat Plate Results

The major effect of the maximum density on the heat transfer can be seen in Figure 7, which is a plot of N_{Nu} against T_∞ for each sphere. The curves are in general agreement with the flat plate results of (*15*) showing a sharp minimum somewhere between 5° and 6°C. Figure 7 lacks utility, however, since the way to estimate a Nusselt number for a sphere of arbitrary diameter is not specified.

In order to pinpoint the effect of diameter, the experimental Nusselt numbers for the spheres have been correlated with the theoretical melting flat plate results of (*15*) by using

$$\frac{N_{Nu}:\text{ flat plate}}{N_{Nu}:\text{ sphere}} = C\left(\frac{L}{D}\right)^{3/4} \qquad (17)$$

If a more general fitting equation such as

$$\frac{N_{Nu}:\text{ flat plate}}{N_{Nu}:\text{ sphere}} = C\left(\frac{L}{D}\right)^{n} \qquad (18)$$

is used, it can be shown from the heat transfer data that 1.0 is a better value for n in the least-squares sense. But the diminution in standard deviation (by using $n = 1$) is quite small, and the value of ¾ allows a complete correspondence with the flat plate results for all diameters. The result for the fitting constant C is 1.106 ± 0.144,* and by using this, the experimental data have been scaled up and plotted in Figure 8.

Physically, Figure 8 means that a melting sphere behaves very similarly to a melting flat plate. From the value of C, if all the transfer parameters are equal (including temperature, characteristic length, and surface area), about 11% more heat is transferred by free convection to the flat plate than to the sphere. This is the effect of curvature on the flow velocities and is in good agreement with Merk's analytical results for nonmelting free convection systems without any maximum density effects [see page 221 of (*9*)] where

$$\frac{N_{Nu}:\text{ flat plate}}{N_{Nu}:\text{ sphere}} = \frac{0.636(N_{Gr}\cdot N_{Pr})^{1/4}}{0.558(N_{Gr}\cdot N_{Pr})^{1/4}} = 1.14\left(\frac{L}{D}\right)^{3/4} \qquad (19)$$

The experimental values between 5° and 6°C. were not included in the fit because the corresponding flat plate results are unknown or unreliable. These results are shown (appropriately scaled) in Figure 8, and they indicate that the minimum Nusselt number for spheres occurs at T_∞ = 5.35 ± 0.2°C. Merk's theoretical result is quoted as 5.31°C. on page 448 of (*8*), although he uses 4.8°C. as a better approximation in (*4*). The lowest experimental value for N_{Nu} was 21.0 (based on a characteristic length of 10.2 cm.), showing that convection effects are always present, since for pure conduction $N_{Nu} = 2$.

It seems reasonable that the correspondence between flat plate and sphere heat transfer will hold for the nonmelting case ($T_w > 0$) with the same value for C. Thus, by using Equation (17) and Tables 5 to 10 of (*16*), the Nusselt numbers for spheres over a wide range of laminar, unidirectional, free convection conditions in water can be calculated. For $T_\infty > 20$°C., or $T_w > 35$°C., further solutions can be readily generated by using the computational techniques of (*16*).

CONCLUSIONS

The experimental work on melting spheres supports the theoretical predictions in two important ways. First, the behavior of the Nusselt number for $T_w = 0$ and $T_\infty < 20$°C. is corroborated, and second, by the use of Tables 5 to 10 of (*16*) and Equation (17), Nusselt numbers for both spheres and flat plates, either melting or nonmelting, can be interpolated with reasonable confidence (± 7%). This applies only within the bounds of unidirectional, laminar flow. Values of N_{Nu} relevant to the split boundary layer ($T_w = 0$°C. only) can be estimated from the experimental results of Figure 8. Finally, the experimental results suggest the importance of a parameter not used in the analytical presentation: a dimensionless group Φ which would give the time required for any degree of melting regardless of changing shape.

ACKNOWLEDGMENT

This work was performed under Grants Nos. DA-AMC-27-021-65-G16 and DA-AMC-27-021-67-G20 of the U.S. Army Cold Regions Research and Engineering Laboratory, Hanover, New Hampshire.

NOTATION

a_0, a_1, a_2 = coefficients in Equation (6)
b_1, b_2 = constants defined by (16)
C = fitting constant in (7) and (17)
C_p = specific heat at constant pressure, cal./g.
D = sphere diameter, cm.
D_{AB} = mass diffusivity, sq. cm./sec.
D_0 = sphere diameter at time t_0, cm.
F_0, F_1 = apparent weight in absolute units
g = acceleration due to gravity, cm./sec.^{2}
$\overline{h}$ = mean heat transfer coefficient, cal./(sq.cm.)(sec.)(°C.)
k = thermal conductivity, cal./(cm.)(sec.)(°C.)
L = plate height, cm.
M = dimensionless melting parameter, $= C_p(T_w - T_\infty)/\Delta H_f$
n = exponent in (18)

* Other fits on various portions of the data are shown in (*16*).

N_{Fo} = Fourier number = $\alpha t/D^2$

N_{Gr} = Grashof number = $\dfrac{g D^3|\beta_\infty(T_w - T_\infty)|}{\nu^2}$

N_{Nu} = average Nusselt number

$N_{Nu_{ex}}$ = experimental Nusselt number = $\bar{h}L/k$

N_{Pr} = Prandtl number = $\mu C_p/k$

N_{Ra} = Rayleigh number = $N_{Gr}N_{Pr}$

N_{Sh} = Sherwood number

Q = total heat transfer to sphere, cal.

t = time, sec.

t_1 = initial time, time of first reliable reading, sec.

t_2 = final time, last reading taken, sec.

T = temperature, °C.

T_f = mean film temperature = $(T_w + T_\infty)/2$, °C.

T_w = wall temperature, °C.

T_∞ = bulk fluid temperature, °C.

V_0, V_1 = volume of ice sphere at times t_0 and t_1, cc.

V_L = volume of lead sinker, cc.

w, W = apparent weight, g.

W_L = weight of lead sinker, cc.

Greek Letters

α = thermal diffusivity, sq. cm./sec.

β_∞ = coefficient of expansion defined in (*12, 15*), (°C.)$^{-1}$

γ = density ratio, ρ_l/ρ_s

ΔC = concentration difference, g./cc.

ΔH_f = latent heat of fusion $(H_l - H_s)$, cal./g.

ϵ = fractional change in radius or diameter = $(D_0 - D_1)/D_0$

μ = viscosity, poise

ν = kinematic viscosity, sq. cm./sec.

ρ = density, g./cc.

ρ_g = gas density, g/cc.

Φ = degree of melting function, defined by (12)

Subscripts

° = evaluated a 0°C., also referring to time t_0

∞ = evaluated far from the wall

l = liquid

s = solid

w = evaluated at the wall

1, 2 = calculated at times t_1, t_2

LITERATURE CITED

1. Bird, R. B., W. E. Stewart, and E. L. Lightfoot, "Transport Phenomena," p. 248, Wiley, New York (1965).
2. "Chementator," *Chem. Eng.*, **74**, 20 (1967).
3. Chiang, T., A. Ossin, and C. L. Tien, *J. Heat Transfer*, **86C**, 4 (1964).
4. Dumore, J. M., H. J. Merk, and J. A. Prins, *Nature*, **172**, 460 (1953).
5. Ede, A. J., *Appl. Sci. Res.*, **A5**, 458 (1955).
6. Koh, J. C. Y., and J. F. Price, *J. Heat Transfer*, **87C**, 2 (1965).
7. Kranse, A. A., and A. J. Schenk, *Appl. Sci. Res.*, **A15**, 397 (1966). Schenk, A. J., and F. A. M. Schenkels, *Appl., Sci. Res.*, **19**, 465 (1968).
8. Merk, H. J., *ibid.*, **A4**, 435 (1954).
9. ———, and J. A. Prins, *ibid.*, 11, 195, 207.
10. Powell, R. W., *Advan. Phys.*, **7**, 276 (1958).
11. "Review of the Properties of Snow and Ice," SIPRE Rept. 4, p. 88, (July, 1951).
12. Schechter, R. S., and H. S. Isbin, *AIChE J.*, **4**, No. 1, 81 (1958); Schechter, R. S., Ph.D. thesis, Univ. Minn., Minneapolis (1956).
13. Tkachev, A. G., *AEC-Tr-3405*, translated from a Publication of the State Power Press, Moscow-Leningrad (1953).
14. Van der Burgh, S., *Appl. Sci. Res.*, **A9**, 293 (1960).
15. Vanier, C. R., and Chi Tien, *Chem. Eng. Progr. Symposium Ser. No. 82*, **64**, 240 (1968).
16. ———, M. S. thesis, Syracuse Univ., N. Y. (1967).
17. ———, and Chi Tien, *Chem. Eng. Sci.*, **22**, 1747 1967).

Manuscript received March 28, 1968; revision received July 23, 1968; paper accepted July 26, 1968.

Mass Transfer in a Nonuniform Impinging Jet

M. T. SCHOLTZ

Toronto Coppersmithing Company Limited, Scarborough, Ontario

and OLEV TRASS

University of Toronto, Toronto, Ontario

Part I. Stagnation Flow-Velocity and Pressure Distribution

A theoretical solution for the impingement flow of a jet with a parabolic velocity distribution is given. Viscous generation and diffusion of vorticity in the jet were neglected. Experimental velocity and pressure distributions measured in an impinging jet of air originating with Poiseuille flow compare well with theory, thus justifying the assumption of inviscid flow. Pressure distributions on the deflecting surface were independent of nozzle height in the range 1 to 12 nozzle radii. For lower nozzle heights the effect of the constriction of flow between the nozzle and the surface followed the predicted behavior.

Impinging jets of fluid are frequently used in industry for heating and cooling operations. In the aero space sciences, special efforts have been made to interpret the behavior of axisymmetric impinging jets with application to vertical take off and landing devices. In applications where heat or mass transfer is of importance, interest in impinging jets is directed to phenomena associated with the region of the viscous boundary layer which develops on the impingement surface.

Figure 1 is a sketch of an axisymmetric impinging jet. The flow in the oncoming jet may be laminar or turbulent; the time average flow may be uniform (left-hand side) or